JOURNAL OF APPLIED ELECTROCHEMISTRY 6 (1976) 211–220

The hydrodynamics of a magnetoelectrolytic cell

S. MOHANTA, T. Z. FAHIDY

Department of Chemical Engineering, University of Waterloo, Canada

Received 15 April 1975

The characteristics of induced flow in a cylindrical magnetoelectrolytic cell under the influence of uniform and non-uniform magnetic fields are analysed. Experimental surface velocity values are predicted with reasonable accuracy by magnetohydrodynamic models incorporating open-channel flow concepts.

Nomenclature

A, D	parameters in Equation 7 [Gak equation]
B	magnetic flux density vector; B_r, B_z its radial and axial components; B_0 its magnitude, $\bar{B}$ its average magnitude
$B_1(pr)$	auxiliary function in the annular Hankel transform technique (Equation 6)
e	unit vectors in the cylindrical coordinate system with components e_r, e_o, e_z
F_θ	magnitude of the MHD force density in the θ-direction
f_c	friction coefficient of energy loss due to curvature
g	acceleration due to gravity
H	height of the electrodes in electrolytic cell
h_f	energy head loss due to friction
h_c	energy head loss due to curvature
I	electric current flow
J	electric current density vector
K	lumped parameter; $K = IB_o/2\pi H\eta$
K_f, K_c	K factors in terms of friction and curvature losses
k	geometric shape factor, R/r_o
P	pressure
p	annular Hankel transform parameter
R	radius of the outer electrode
r_o	radius of the inner electrode
r	radius measured from the centre of the electrolytic cell
V_θ	velocity in the θ-direction; $\bar{V}_\theta$ its average
α_n	regression coefficients in Equation 13
η	dynamic viscosity of electrolyte
ν	kinematic viscosity of electrolyte
ρ	density of electrolyte
$\phi(p)$	function defined in Equation 8a
$\psi(r)$	surface profile function (Equation 29)

1. Introduction

It is well known in the theory of fluid dynamics that some flow systems of cylindrical geometry can be successfully analyzed in terms of unidimensional models [e.g., 1, 2]. From a magnetohydrodynamic (MHD) point of view, cylindrical cells are particularly inviting systems to study: if the electric field is radial and the magnetic field is axial, the resulting fluid bulk motion is tangential (azimuthal), and if the electrode surface is free, its curvature between the electrodes can be estimated by unidimensional approximations. The purpose of this paper is to present the results of a thorough analysis [3] of a cylindrical cell in magnetoelectrolysis with emphasis on the application of the concepts of open channel flow theory to the hydrodynamics of the electrolytic cell.

The cell geometry is shown in Fig. 1; if the total

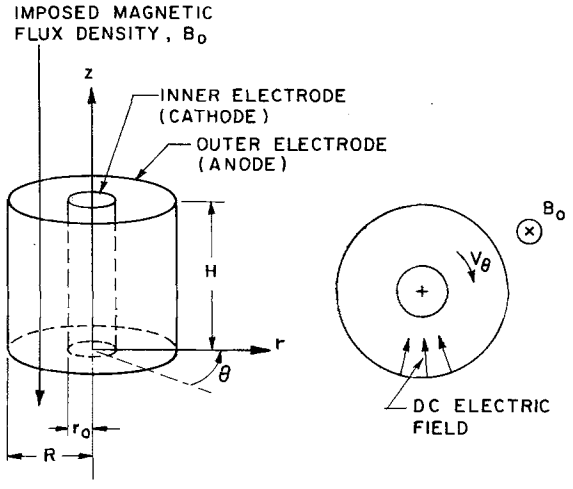

Fig. 1. Coordinate system in the cylindrical cell.

I is uniformly distributed in the axial (z) direction, then the radial current density is obtained from the current balance div $J = 0$ as

$$J = e_r \frac{I}{2\pi Hr}. \tag{1}$$

If a magnetic field of flux density $B = e_r B_r - e_z B_z$ is imposed upon the radial electric field, a MHD body force is generated, with density

$$J \times B = -e_\theta \frac{IB_z}{2\pi Hr} \tag{2}$$

resulting in a tangential motion around the cylindrical annulus.

Equations 1 and 2 are the fundamental relationships governing cylindrical cells in magneto-electrolysis, when $J_\theta = J_z = B_\theta = 0$.

2. Theoretical

In a uniform magnetic field ($\mathbf{B} = -e_z B_o$) the MHD body force acts only in the θ-direction and the generated motion is tangential to the electrodes. If $V_r = V_z = 0$ is assumed, from continuity considerations the equation of motion in the steady state may be written as follows:

r-component: $$\rho \frac{V_\theta^2}{r} = \frac{\partial P}{\partial r} \tag{3a}$$

θ-component: $$\eta \frac{r}{\partial r}\left[\frac{1}{r}\frac{\partial}{\partial r}(rV_\theta)\right] + \eta \frac{\partial^2 V_\theta}{\partial z^2} = -F_\theta \tag{3b}$$

z-component: $$-\frac{\partial P}{\partial z} = \rho g. \tag{3c}$$

Here, $F_\theta = \frac{IB_o}{2\pi Hr} = \frac{K\eta}{r}$ is the MHD body force density and K is a lumped parameter defined as $K \equiv \frac{IB_o}{2\pi H\eta}$. The boundary conditions $r = r_o$: $V_\theta = 0$; $r = R$: $V_\theta = 0$; and $z = 0$: $V_\theta = 0$, for solving Equation 3b, have to be supplemented by an additional condition related to the air-electrolyte interface. Since the surface velocity profile is indeterminate without the prior knowledge of V_θ, a rigorous solution is not feasible. One rational approximation is that on the free surface the axial derivative of V_θ is a single, *a priori* unknown, r-dependent function:

$$z = H: \frac{\partial V_\theta}{\partial z} = F(r). \tag{4}$$

Then, Equation 3b can be solved via the Annular Hankel Transformation technique [4] to yield

$$V_\theta(r, z) = \frac{\pi^2}{2} \sum_p \frac{p^2 J_1(pR)}{J_1^2(pr_o) - J_1^2(pR)} B_1(pr) V_h \tag{5}$$

where

$$V_h = \frac{KN(p)}{p^2}[1 - \cosh(pz)] + \frac{\sinh(pz)}{p\cosh(pH)}\left[F(p) + \frac{KN(p)}{p}\sinh(pH)\right]$$

$$N(p) = \frac{1}{p} Y_1(pr_o)[J_0(pr_o) - J_0(pR)] - \frac{1}{p} J_1(pr_o)[Y_0(pr_o) - Y_0(pR)]$$

$$F(p) = \int_{r_o}^{R} rF(r) B_1(pr)\, dr$$

$$B_1(pr) = Y_1(pr_o)J_1(pr) - Y_1(pr)J_1(pr_o) \tag{6}$$

p are the positive roots of the equation $B_1(pR) = 0$, in an increasing order. One can distinguish between the following specific cases:

(1) The axial variation of V_θ is neglected; the solution of Equation 3b is carried out with the two 'standard' boundary conditions stated above, $V_\theta = 0$; $r = R$ and $r = r_o$. Gak [5] treated this problem in terms of the classical Euler equation and obtained the solution in the form of

$$V_\theta = K\left(A_r - \frac{D}{r} - r\log_e r\right) \tag{7}$$

where

$$A \equiv \log_e R + \frac{r_o^2 \log_e R/r_o}{R^2 - r_o^2}$$

$$D \equiv \frac{r_o^2 R^2 \log_e R/r_o}{R^2 - r_o^2}.$$

An alternative and numerically identical solution is obtained from Equation 5 upon proper simplifications:

$$V_\theta = \frac{K\pi^2}{2} \sum_p \phi(p) \tag{8}$$

$$\phi(p) \equiv \frac{J_1^2(pR) B_1(pr) N(p)}{J_1^2(pr_o) - J_1^2(pR)}. \tag{8a}$$

The appendix contains further details, the first ten roots of Equation 6 and the corresponding numerical values of $\phi(p)$.

(2) The free surface is assumed to be flat; momentum transport to the air-liquid interface is relatively small. In this instance

$$\frac{\partial V_\theta}{\partial z} = F(r) = 0. \tag{9}$$

Then, $F(p)$ is also zero and Equation 5 is simplified to

$$V_\theta(r, z) = \frac{K\pi^2}{2} \sum_p \frac{J_1^2(pR)}{J_1^2(pr_o) - J_1^2(pR)} \times B_1(pr)N(p)f(p, z) \tag{10}$$

where

$$f(p, z) = 1 - \cosh(pz) + \tanh(pH)\sin(pz). \tag{11}$$

Note that if $f(p, z) = 1$, Case (1) is obtained.

(3) Straight open channel with Owen's boundary condition replacement. Owen [6] has shown that the boundary condition in a straight open channel can be transformed to that of a closed conduit of twice the height of an open channel. Thus, one has

$V_\theta = 0$ at $r = R$ and r_o; at $z = 0$ and $z = 2H$

where it follows that Equation 10 is once again the solution of the velocity distribution equation, with

$$f(p, z) = 1 - \cosh(pz) + [\cosh(2pH) - \operatorname{cosech}(2pH)]\sinh(pz). \tag{12}$$

If the (pH) argument is relatively large, Equations 11 and 12 become essentially identical.

3. Experimental

The MHD behaviour of an experimental cylindrical cell with $CuSO_4/H_2SO_4$ electrolytes was studied [3] in an apparatus described previously [7, 8]. The electrodes were 99·9% pure copper. The proper roundness of the electrodes was checked after fitting them into circular grooves in the bottom plate of the cell and the diameters were found to vary within 0·25% of the average diameter; the cylindrical cell was made of plexiglass with three grooves of different size to hold the electrodes in place. The backsides of the electrodes (not facing each other) were insulated from the electrolyte. Two cells were operated in this manner: (a) the 'inner' cell with $r_o = 1{\cdot}43$ cm, $R = 5$ cm, and (b) the 'outer' cell with $r_o = 5$ cm, $R = 10{\cdot}5$ cm; all electrodes had a height of 4·45 cm (inner cell) and 3·81 cm (outer cell). The inner cell was situated within the highly homogeneous zone between the magnet pole faces, whereas the outer cell occupied a zone beyond the pole faces. This arrangement allowed operation in a non-uniform magnetic field, whose flux density-radius (measured from the centre of the pole faces, i.e., the centre of the cylindrical cells) relationship was correlated via regression analysis as

$$B(r) = \sum_{n=1}^{N} \alpha_n r^n. \tag{13}$$

The α_n coefficients were found to depend on the magnitude of the exciting current and are shown in Table 1.

The velocity of the free surface of the electrolyte was measured by observing the time required

Table 1. Values of the coefficients in Equation 13 for various magnet-exciting current flows ($N = 5$)

Magnet-exciting current (A)*	*Values of* α_n					
	$n = 1$, Tm^{-1}	$n = 2$, Tm^{-2}	$n = 3$, Tm^{-3}	$n = 4$, Tm^{-4}	$n = 5$, Tm^{-5}	$\bar{B}$, T†
0	0·363	− 12·72	215·75	− 1772·5	5513·9	0·0031
10	7·070	− 208·64	3137·10	− 23929·0	70042·0	0·0814
20	22·767	− 884·74	16595·00	−130872·0	408790·0	0·1640
40	30·371	−1004·30	16595·00	−135847·0	423971·0	0·3067
60	32·136	− 752·41	9115·70	− 59797·0	152270·0	0·4466
96	61·090	−1910·40	30341·00	−242031·0	736922·0	0·6563

* Total active range: 0–98 A.
† See Equation 23 for definition.

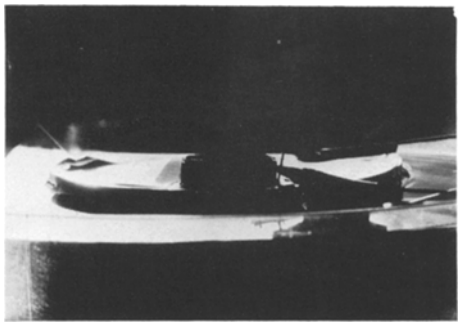

Fig. 2. Electrolyte surface during magnetoelectrolysis. Run 215, inner cell. $I = 336{\cdot}8$ mA, $B = 0{\cdot}78$ T.

for a light particle of about 0·5 mm diameter to complete a certain number of revolutions around the inner electrode, at a noted radial position. 'Still' photographs of the surface were taken at various cell current densities and magnetic flux densities; a typical surface profile is shown in Fig. 2 for the inner cell.

4. Results and discussion

4.1. *Velocity profile at surface*

In comparing theory to the experimental findings in this work, Figs. 3 and 4 give a preliminary indication of the degree of agreement expected. In Fig. 3 the velocity versus fractional height distributions, predicted by Equations 7, 10, 11 and 12, are compared, for the radial position $\frac{1}{2}(R + r_o)$. In Fig. 4 the radial distribution of V_θ on the surface is plotted via these equations, together with the range of the experimentally observed particle paths $r = r_p$. Equation 7 predicts an axially independent motion; the other equations predict essentially identical profiles but the surface velocity ($z/H = 1$) is 5% smaller than predicted by Equation 7. It is important to note, however, that the experimentally observed values of V_θ are 50–90% lower than the theoretical predictions, as shown in Fig. 5 for two distinct particle paths (2·9 and 3·81 cm). While such a large disagreement is not surprising *per se* (e.g., Gak's experimental data also show serious disagreement between Equation 7 and his findings [5]), its existence clearly indicates that the hitherto presented theoretical models, no matter how mathematically complex they are, apply only as a crude approximation.

We shall now propose a more advanced theory and show its good agreement with experimental evidence. It is essentially an open-channel hydraulic model: the MHD force density being horizontal, it is parallel to the bottom of the cell (i.e., channel) and flow in the electrolytic cell is considered to be analogous to open channel flow with the bottom of the channel having a slope

$$S = \frac{F_\theta}{F_z} = \frac{JB}{\rho g} = \frac{K\eta}{\rho g r} \qquad (14)$$

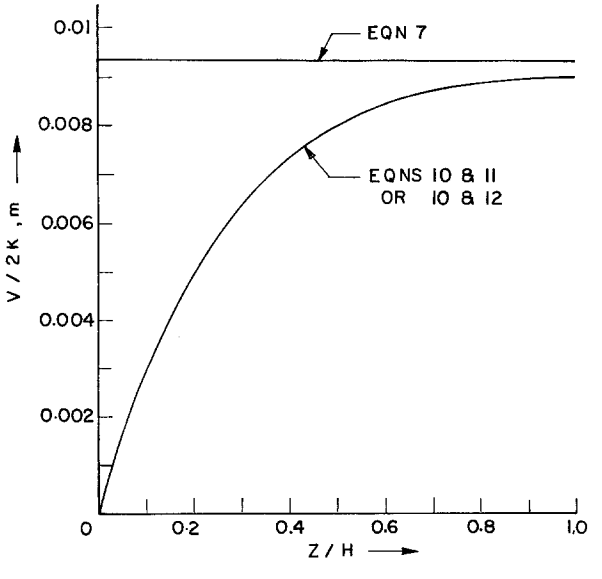

Fig. 3. The axial distribution of V_θ estimated by Equations 7, 10, 11 and 12, at $r = (R + r_o)/2$.

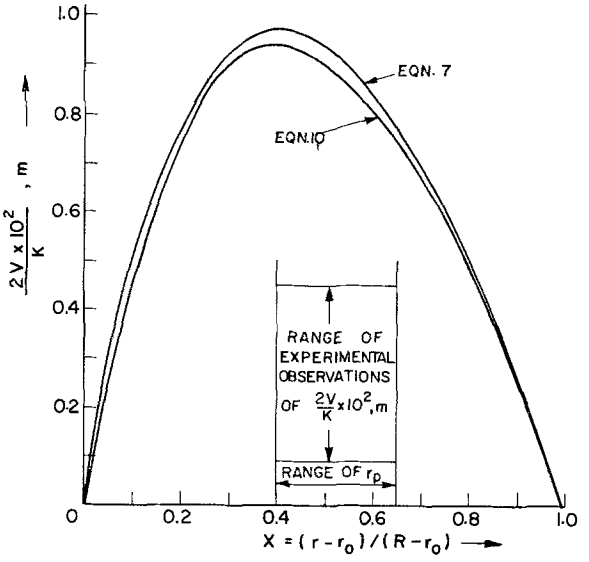

Fig. 4. The theoretical radial distribution of V_θ and the range of observations at $z = H$.

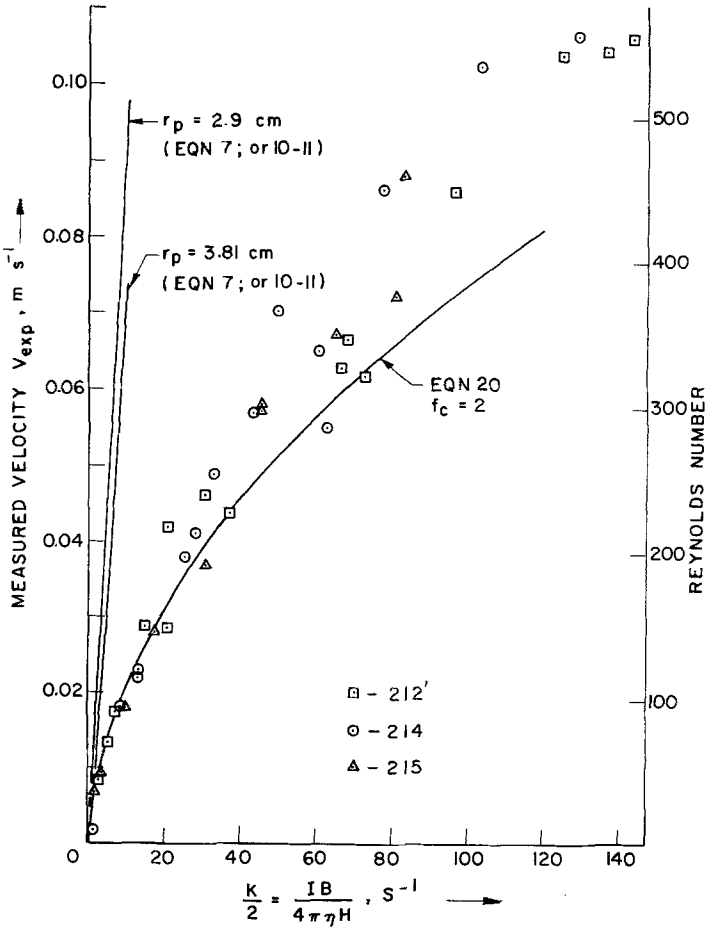

Fig. 5. Experimental surface velocities and theoretical predictions, inner cell.

with an average value of $S_{ave} = [2K\eta/\rho g(R + r_o)]$. Experimental evidence indicates that the electrolyte surface is curved. This curvature is caused by the presence of a centrifugal force generated by the MHD body force. In addition to the frictional loss one would expect a loss of fluid energy due to the bend [8–11]. If, therefore, this loss can be estimated in a rational manner, the surface curvature and velocity estimates should be less approximate in nature than those normally set by restrictive boundary conditions.

At present, there seem to be only 'rule of thumb' approaches to estimating the energy loss in fluids due to curvature in open channel laminar flow [8, 9]. Shukry [10] recommends for $Re >$ 10 000 a head loss estimate $h_c = f_c V^2/2g$ where f_c depends on Re and other parameters. It is usual practice to assume a loss of $(\bar{V}_\theta^2)/2g$ for a 90° bend [11], and 1·4 times this value for a 180° bend [12]. One would be inclined to take a factor of 2 for a 360° bend which is the case of a cylindrical cell. In a more refined analysis, taking Equation 14 and $2\pi r$ as the path length for this slope, the available liquid head would be $h_t = 2\pi K\nu/g$ and the friction loss and curvature loss would be computed in the following manner.

Assume that the velocity distribution is given by the combination of Equations 10 and 11, and since the first root of Equation 6 is strongly dominant (see Table A1 in Appendix), a single term expansion is sufficient. Then,

$$V_\theta \cong \frac{K_f}{2}\left[Ar - \frac{D}{r} - r\log_e r\right] \times [1 - \cosh(p_1 z) + \tanh(p_1 H)\sinh(p_1 z)] \quad (15)$$

where K_f is equivalent to the energy needed to overcome the friction loss (loss due to curvature *not* included). The average velocity, upon integration of Equation 15, can be written as

$$V_\theta \cong K_f r_o f(k)\left[1 - \frac{\tanh(p_1 H)}{p_1 H}\right] \quad (16)$$

where

$$f(k) = \frac{(k+1)(k^3-1) - 6k^2\log_e k}{9(k^2-1)(k+1)}; \quad k = R/r_o. \quad (17)$$

Hence, the energy required to overcome (1) the friction loss is

$$h_f \cong \frac{2\pi K_f \nu}{g} = 2\pi\frac{\nu}{g}\frac{\bar{V}_\theta}{r_o f(k)}\frac{p_1 H}{p_1 H - \tanh(p_1 H)}, \quad (18)$$

and (2) the curvature loss is

$$h_c = \frac{2\pi K_c \nu}{g} = f_c\frac{\bar{V}_\theta^2}{2g}. \quad (19)$$

f_c is to be found experimentally. The total loss in energy is

$$h_T = h_f + h_c \quad (20)$$

and if one sets $K = K_f + K_c$, Equation 20 can be expressed in the more convenient form of

$$\frac{K}{2} = \frac{\bar{V}_\theta}{2r_o f(k)}\frac{p_1 H}{p_1 H - \tanh(p_1 H)} + \frac{f_c}{8\pi\nu}\bar{V}_\theta^2 \quad (21)$$

which is the relationship between the average velocity and the MHD body force density. The relationship between the surface velocity and average velocity can now be established by computing the value of V_θ at $z = H$ via Equations 10–12, and the value of $\bar{V}_\theta$ by appropriate integrals of these equations. The result of this computation is the simple, but approximate expression

$$\bar{V}_\theta \cong 0{\cdot}526\, V_\theta|_{z=H} \quad (22)$$

where $V_\theta|_{z=H}$ is an estimate of the experimentally measured surface velocity, v_{exp}. The two quantities are compared in Fig. 5, where the solid curve was constructed via Equations 21 and 22, using $f_c = 2$. Fig. 5 also contains predictions via Equations 7 or 10–11 and as seen, the theory utilizing open-channel flow concepts with bend loss taken into account yields much better estimates of the surface velocity at low and medium magnetic flux densities, than otherwise. However, as $Re = 500$, the onset of transition flow in open-channel hydraulics is approached, the discrepancy between experimental and predicted surface velocity becomes appreciable. One possible reason for this disagreement is the effect of Re on the friction parameter f_c; as shown by Shukry [10], f_c sharply decreases as Re increases from 10^4 to $4{\cdot}10^4$. It is quite possible that the inverse effect of Re on f_c becomes gradually manifest as the flow ceases to be laminar and both average velocity and surface velocity become larger for a given value of K. In view of the apparent lack of any reliable method to estimate the $f_c(Re)$ relationship in the

transition zone for the experimental cell, no further analysis of this set of observations has been made so far.

In the inhomogeneous magnetic field, $F_\theta = \dfrac{IB(r)}{2\pi H\eta r}$ and $B(r)$ is given by Equation 13. A rigorous solution of Equation 3b, if possible at all, would be rather tedious. If the z-dependence of V_θ is neglected, the solution, written as

$$\frac{V_\theta}{K_1} = -\sum_{n=1}^{N} \frac{\alpha_n r^{n+1}}{n(n+2)} + \frac{r}{R^2 - r_o^2} \sum_{n=1}^{N} \frac{\alpha_n}{n(n+2)} (R^{n+2} - r_o^{n+2}) + \frac{r_o^2 R^2}{r(r_o^2 - R^2)} \sum_{n=1}^{N} \frac{\alpha_n}{n(n+2)} (R^n - r_o^n) \quad (23)$$

$$K_1 = \frac{I}{2\pi H\eta}$$

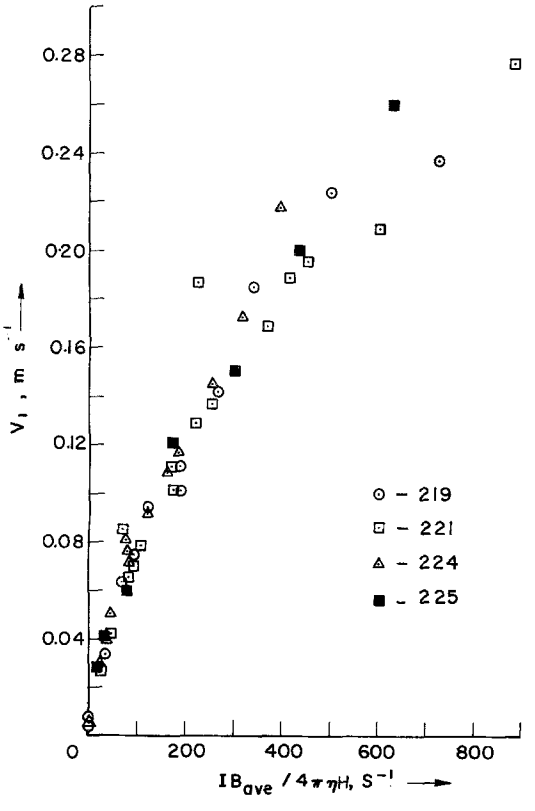

Fig. 6. Plot of experimental velocity versus the $IB/4\pi\eta H$ group, outer cell.

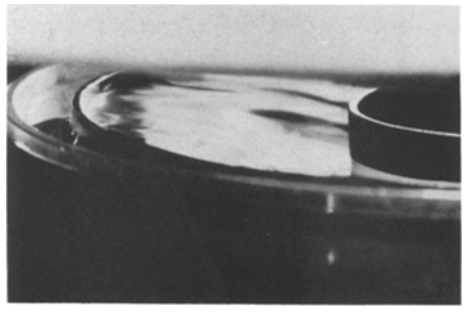

Fig. 7. Electrolyte surface during magnetoelectrolysis. Magnet-exciting current flow = 96 mA. I = 3·282 A, outer cell. Note the ripples on the electrolyte surface.

replaces Equation 9 or Equations 9–11. The development of an open-channel flow relationship (i.e., a counterpart of Equation 21) would also be rather cumbersome and is beyond the scope of this investigation. Some simplification, however, can be effected by considering the average, or equivalent homogeneous magnetic flux density which is computed as

$$\bar{B} = \frac{1}{A_c} \int_{A_c} B(r)\,dA_c \quad (24)$$

where A_c is the channel surface area; $\bar{B}$ is a function, of course, of the magnet-exciting current flow, as shown in Table 1.

Fig. 6 shows the effect of the average MHD body force density on the experimentally observed surface velocity in a nonhomogeneous magnetic field, using the 'outer' cell. In Fig. 7 a photograph of the electrolyte surface is shown at a relatively large d.c. current flow and the strongest magnetic field gradient attained in the experimental apparatus: notice the ripples on the electrolyte surface whose growth with a gradual increase in the electric field strength ultimately leads to instability (electrolyte spills over the electrode). Thus, in a nonhomogeneous magnetic field severe turbulence can be generated via magnetoelectrolysis. The relationship between velocity and the MHD body force can be written, via open-channel flow theory, as

$$\frac{K}{2} = \frac{V^2}{8\pi\nu}\left(f_c + f_p \frac{L}{D_h}\right) \quad (25)$$

where f_p is the turbulent head loss coefficient and D_h is the hydraulic diameter. Since velocity measurements under fully turbulent conditions

could not be carried out with reliable accuracy, no attempt has been made to plot Equation 25 on Fig. 6. Research into this aspect of the cell hydrodynamics would be an interesting area of study.

4.2. *Estimation of the surface profile*

It was shown in the previous section that the electrolyte surface becomes curved under properly chosen conditions of the magnetic/electric field coupling. The curvature effect can be estimated in the laminar flow regime from the pressure distribution across the cell, in the following manner.

From Equations 3a and c, upon integrating the total pressure differential, one obtains

$$P - P_a = \rho[f_1(r,z) - f_2(R,z)] - \rho g(z - z_R) \tag{26}$$

where P_a is the (reference) atmospheric pressure, taken at the outer electrode ($r = R$) where the electrolyte surface height is z_R. The f_1 function is defined as

$$f_1(r,z) = \int_{r_0}^{r} \frac{V_\theta^2}{r}\, dr. \tag{27}$$

The free surface profile is obtained when $P = P_a$, thus at any radial position r, the electrolyte surface height is given as

$$z_r = z_R - \frac{f_1(R,z_r) - f_1(r,z_R)}{g}. \tag{28}$$

An estimate of the $z_r(r)$ function may be established if a simple velocity distribution is assumed, such as

$$V_\theta = K'\left(r \log_e \frac{R}{r} - \frac{r_o^2}{r} \log_e \frac{R}{r_o} \frac{R^2 - r^2}{R^2 - r_o^2}\right) \tag{29}$$

where K' is an experimental K-factor; Equation 29 is a slightly modified version of Equation 7. Thus, a z-independent approximation to Equation 27 may be computed, as in Fig. 8 which shows a typical surface profile for the inner cell. Here, the quantity

$$\frac{(z_R - z_r)g}{(K')^2} = \psi_1(R) - \psi_1(r) \tag{30}$$

was plotted against the fractional cell width. ψ_1 is the integral on $[r_o, r]$ of the square of the bracketed term in Equation 29, upon division by r. The

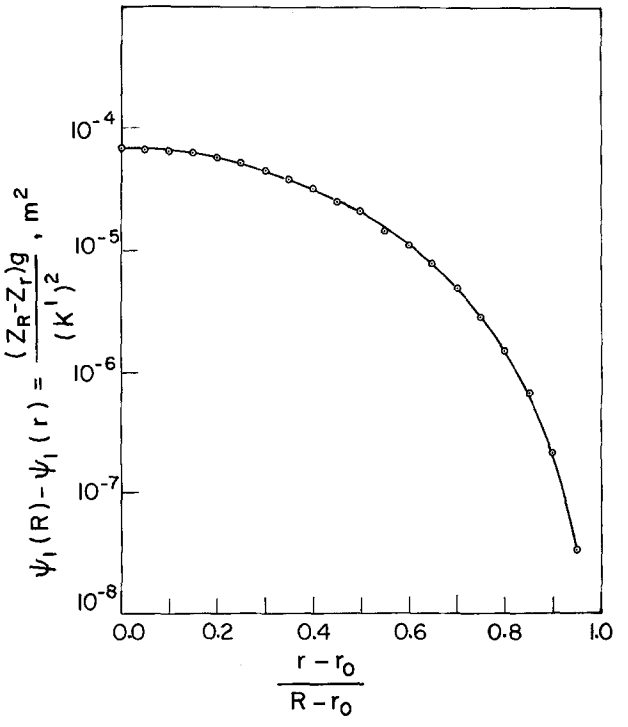

Fig. 8. Surface profile predicted via Equation 30.

magnitude of $(z_R - z_{r_o})$ is of the order of a few mm according to Equation 30 and Fig. 8, which agrees with corresponding experimental observations.

4.3. *The effect of cell geometry*

The preceding analysis indicates that the cell geometry has a direct bearing on the MHD behaviour of the cell. Indeed, the surface velocity reaches a maximum at a radial position $r_o < r_{max} < R$, whose approximate value is obtained via differentiation of Equation 7 or 28:

$$\log_e \frac{R}{r_o} \cdot \frac{R^2 - r_{max}^2}{R^2 - r_o^2} = \frac{r_{max}^2}{r_o^2} + \frac{r_{max}^2}{R^2 - r_{max}^2} \quad (31)$$

r_{max} does not depend on the strength of the imposed magnetic field but it strongly depends on the aspect ratio k. The value of r_{max} is 2·89 cm for the experimental cell ($k = 3{\cdot}643$); if the outer electrode radius were doubled, r_{max} would be 4·67 cm for $R = 10{\cdot}2$ cm and so forth. Moreover, the corresponding fractional width values would slowly decrease and the relative position of the maximum velocity would tend toward the inner electrode.

The effect of the electrode height is also important. For a given k, the higher the electrode height, the less marked the axial distribution of the electrolyte velocity, and the more accurate the unidimensional r-dependent flow model. Conversely, if the electrodes are short, bottom and edge effects become relatively important and the foregoing analysis would not apply.

5. Concluding remarks

This study has shown that the MHD flow in a magnetoelectrolytic cell can be successfully analysed by means of open-channel flow hydraulics and the surface velocity can be predicted at a reasonably good accuracy in the laminar regime by accounting for (1) the friction loss of fluid energy at the cell walls and (2) the energy loss due to curvature. The understanding of the pertinent MHD behaviour permits the design of magneto-electrolytic cells with desired flow characteristics.

Acknowledgment

This project was supported by the National Research Council of Canada.

References

[1] F.A. Holland, *Fluid Flow for Chemical Engineers*, E. Arnold, 1973, Chapter 14.
[2] N. Curl and H.J. Davies, *Modern Fluid Dynamics*, Van Nostrand, 1968, Volume 1, Section 5.3.
[3] S. Mohanta, Ph.D. Thesis, Univ. of Waterloo, 1974.
[4] C.J. Tranter, *Integral Transforms In Mathematical Physics*, Methuen 1962, pp. 88–91.
[5] E.Z. Gak, *Elektrokhimiya* 3 (1967) 89.
[6] W.M. Owen, *Trans. Am. Soc. Civ. Engrs.* 119 (1954) 1157.
[7] S. Mohanta, M.A.Sc. Thesis, Univ. of Waterloo, 1971; S. Mohanta and T.Z. Fahidy, *Can. Journ. Chem Engrg.* 50 (1972), 248.
[8] *Handbook of Applied Hydraulics*, ed. by C.V. Davis and K.E. Soresmen, McGraw Hill, 1969.
[9] H.M. Morris and J.M. Wiggert, *Applied Hydraulics in Engineering*, Ronald Press, 1972.
[10] A. Shukry, *Trans. Am. Soc. Civ. Eng.* 115 (1950) 751.
[11] E.H. Lewitt, *Hydraulics and Fluid Mechanics*, 10th edn, Pitman and Sons, 1958, p. 107.
[12] *Chemical Engineer's Handbook*, ed. by J.H. Perry, McGraw Hill, 1963.
[13] I.N. Sneddon, *Phil. Mag.* 7 (1946) 17.
[14] E. Jahnke and F. Emde, *Table of Functions*, Dover, 1945, Chapter 8.
[15] M. Abramowitz and I.A. Stegun, *Handbook of Mathematical Functions*, Dover, 1965, Chapters 9, 10, 11.
[16] H.E. Fettis and J.C. Castin, 'An Extended Table of Zeros of Cross Products of Bessel Functions', ARL 66-0023, Feb. 1966; Dec. 1968.

Appendix

1. Summary of the annular Hankel transform (AHT) technique

This approach of operational calculus has been discussed by Sneddon [13] and summarized by Tranter [4]. The transform is especially useful in treating the differential operator

$$L(r) = \frac{1}{r}\frac{\partial}{\partial r}\left(r\frac{\partial V}{\partial r}\right)$$

of fluid dynamics in cylindrical and spherical coordinate systems. The AHT of a function $f(r)$ is

defined as

$$f(p) \equiv \int_{r_0}^{R} rf(r)B_n(pr)\mathrm{d}r; \quad R > r_0 \qquad \text{(A1)}$$

where

$$B_n(pr) = J_n(pr)Y_n(pr_0) - Y_n(pr)J_n(pr_0). \qquad \text{(A2)}$$

J and Y are Bessel functions of the first kind of order n, and p are the positive roots in an increasing order (k = 1, 2, . . .) of the equation

$$J_n(pR)Y_n(pr_0) = Y_n(pR)J_n(pr_0). \qquad \text{(A3)}$$

The inversion formula is given by

$$f(r) = \frac{\pi^2}{2}\sum_{p}\frac{p^2J_n^2(pR)}{J_n^2(pr_0) - J_n^2(pR)}B_n(pr)f(p). \qquad \text{(A4)}$$

If, therefore, Equation 3b is subjected to annular Hankel transformation, the ordinary differential equation

$$\frac{\mathrm{d}^2V(p,z)}{\mathrm{d}z^2} - p^2V(p,z) = -KN(p) \qquad \text{(A5)}$$

is obtained, where

$$N(p) = \int_{r_0}^{R} B_1(pr)\mathrm{d}r;$$

the integrated form is given below Equation 5 in the text. The solution of Equation A5 consists of the homogeneous part $C_1\cosh(pz) + C_2\sinh(pz)$, and of the particular integral $KN(p)/p^2$. Applying the set boundary conditions, the unknown constants C_1 and C_2 may be determined and solutions pertaining to various physical conditions c can be obtained.

2. The roots of Equation 6 and the $\phi(p)$ function

Equation 6 is a special case of Equation A2, when $n = 1$ and $r = R$. The roots p_k, k = 1, 2, 3, . . . , may be obtained by using extensive Bessel function tables [14, 15], or more invitingly for fast electronic computation, by the method of Fettis and Caslin [16], combined with a standard Newton-Raphson root-finding technique. Table A1 contains the numerical values of p_k and the corresponding numerical values of $\phi(p_k)$ in Equation 8 for the first ten indices, computed via the Fettis-Caslin procedure.

Table A1. The first ten roots of Equation A2 for n = 1, r = R_o and the corresponding $\phi(p_k)$ functions. r_o = 1·4 cm; R = 5·1 cm

k	p_k (cm^{-1})	$10^4.\phi(p_k)$ (cm))
1	0·930 95	1003·430
2	1·726 90	− 4·801
3	2·566 99	− 44·112
4	3·414 27	1·577
5	4·257 63	9·429
6	5·104 76	− 0·703
7	5·952 43	− 3·266
8	6·800 45	0·389
9	7·648 71	1·424
10	8·497 13	− 0·245